**COVER SHEET**

*NOTE: This coversheet is intended for you to list your article title and author(s) name only*

*—this page will not appear on the CD-ROM.*

Paper Number: **2712**

Title: **Molecular Dynamics Modeling of Carbon Nanotube Composite Fracture using ReaxFF**

Authors: Benjamin D. Jensen[1]
Kristopher E. Wise[1]
Gregory M. Odegard[2]

**ABSTRACT**

Carbon nanotubes (CNTs) are well known to have exceptionally high mechanical properties when measured individually. Recently, CNT fiber composites have been enabled by the production of high-tex yarns in quantities on the order of kilometers. These high-tex CNT yarns have recently become comparable in specific stiffness and specific strength to carbon fiber. Despite these advancements, CNT yarns still have mechanical properties substantially lower than their CNT constituents. Closing this gap requires understanding load transfer between CNTs and the role of matrix binders such as amorphous carbon at the nanoscale. This work uses reactive molecular dynamics simulations to gain a nanoscale understanding of the key factors of CNT nanocomposite mechanical performance and to place more realistic upper bounds on the target properties.

While molecular dynamics simulations using conventional force fields can predict elastic properties, the ReaxFF reactive force field can also model fracture behavior because of its ability to accurately describe bond breaking and formation during a simulation. The upper and lower bounds of CNT composite properties are investigated by comparing systems composed of CNTs continuously connected across the periodic boundary with systems composed of finite length CNTs. These lengths, effectively infinite for the continuous tubes and an aspect ratio of 13 for the finite length case, result from simulation limitations. Experimentally measured aspect ratios are typically on the order of 100,000, so the calculated results should represent upper and lower limits on experimental mechanical properties. Finally, the effect of various degrees of crosslinking to the amorphous carbon matrix is considered in an attempt to identify the amount of CNT-matrix covalent bonding that maximizes overall composite properties.

---

[1] Advanced Materials and Processing Branch, NASA Langley Research Center, Mail Stop 226, Hampton, VA, 23681-2199

[2] Department of Mechanical Engineering - Engineering Mechanics, Michigan Technological University, 1400 Townsend Dr., Houghton, MI, 49931

## INTRODUCTION

The high strength and stiffness of carbon nanotubes (CNTs) make them promising candidates as reinforcements in structural composites. The recent commercialization of CNT yarns and sheets has enabled the creation of high volume fraction CNT composites where the load is transferred directly between CNTs. Therefore, optimizing load transfer between CNTs is crucial to maximizing the mechanical properties of CNT yarns, matts, and their composites. Computational modeling can be used to provide a detailed description of the load transfer mechanisms and the influence of atomic structure on mechanical properties. However, the aspect ratios of CNTs are on the order of 100,000 with lengths on the order of 1 mm [1-2], which is beyond the practical size of molecular dynamics (MD) simulation methods. Because of this, MD models often approximate CNTs as a continuous molecule, by bonding the CNT to itself across a periodic boundary. Mechanical properties computed using continuous CNTs exceed those expected from experimental materials, which are composed of discontinuous CNTs. The results presented here compare elastic and fracture properties of CNT composite models composed of either continuous or discontinuous CNTs. The continuous CNT models represent a maximum case, while the limited aspect ratio of the discontinuous CNTs modeled here make them a minimum case.

In this work, CNT/amorphous carbon (AC) composite systems composed of discontinuous and continuous CNTs are compared using MD simulations with the reactive force field ReaxFF [3-4]. The objective is to establish a range of mechanical properties using the limiting cases of continuous and small aspect ratio discontinuous CNTs. All systems are composed of two bundles of seven CNTs. The CNTs are covalently crosslinked to the matrix to varying degrees to understand their influence on load transfer for the two system types. The full elastic stiffness tensor is computed and used to derive engineering constants such as Young's modulus. Tensile fracture in the axial direction was also investigated from which the ultimate stress is determined.

## COMPUTATIONAL DETAILS

The systems studied herein were investigated using MD simulations using the reactive force field ReaxFF, as implemented in the molecular dynamics software LAMMPS [5-6]. ReaxFF is a bond-order force field in which the bond order is related to interatomic distances allowing bond breaking and formation to be accurately simulated. See reference [7] for a recent review of the ReaxFF method. Because no significant charges formed in the systems, all charges were set to zero and the charge equilibration scheme disabled resulting in a substantial increase in the simulation speed. The $\text{ReaxFF}_{\text{C-2013}}$ carbon parameterization of Srinivasan *et al.* is used in this work [4]. The $\text{ReaxFF}_{\text{C-2013}}$ parameters have been extensively characterized against both experimental and density functional theory (DFT) computationally determined elastic and fracture properties of diamond, graphene, amorphous carbon, and carbon nanotubes [8]. Images were rendered using the open source Ovito program [9] and color mapping scheme viridis from the software matplotlib version 2.0 [10].

The two system types, composed of continuous and discontinuous CNTs, are shown in Figure 1. The first system type, shown in Figure 1(a), is composed of CNTs of length 10.2 nm that are continuous across the periodic boundary. The second system type, shown in Figure 1(b) is composed of discontinuous CNTs of length 20.1 nm, terminated with hemispherical end-caps. The ends of each CNT are separated by a 2 nm gap that is filled with matrix atoms. The discontinuous CNTs have an aspect ratio of ~13 and an axial simulation box length of 24.1 nm. All CNTs have chirality of (20,0) and a diameter of ~1.56 nm. For discontinuous systems, the CNTs are systematically translated in the axial direction in order to increase the separation between neighboring CNT ends. The length of the CNTs in the discontinuous systems are longer than those in the continuous systems in order to achieve a more reasonable aspect ratio, and to allow for larger spacing between CNT ends.

Each system was subdivided into constituents, as shown in Figure 1, for analysis purposes. As will be discussed later, structuring in the matrix at the CNT interface resulted in substantially different mechanical properties in the interface zone than the bulk matrix. Therefore, the AC matrix constituent was subdivided into an interface layer and bulk matrix.

The effects of covalent bonding between the CNTs and the AC matrix, herein referred to as crosslinking, were also investigated. For each of the two system types (continuous and discontinuous), five models were created with crosslinking fractions near 0%, 5%, 10%, 15%, and 20%. These correspond to number densities of approximately 0.0, 1.9, 3.8, 5.7, and 7.6 crosslinks/nm$^2$. A very small amount of crosslinking of 0.1%-0.4% is present in the lowest crosslink samples and are therefore referred to as <1% crosslink systems.

Examples of crosslinks are shown in Figure 2(a) and Figure 2(b) for 4% and 19% crosslinked discontinuous systems, respectively. Crosslinks between the CNTs and AC matrix are mostly composed of a single $sp^2$ carbon atom, with one covalent bond to a CNT atom and two covalent bonds to matrix atoms. In some cases, the crosslink is an sp bonded atom, often when the geometry of the system restricts access to a second AC atom such as in the crevasse between two CNTs. Crosslinked CNT atoms are majority $sp^3$ content. In some cases, particularly for the

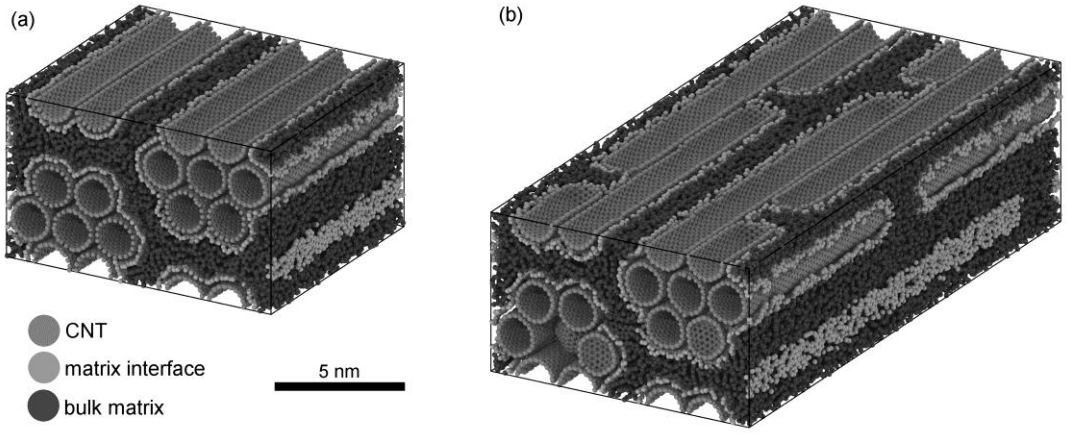


Figure 1 –Equilibrated systems composed of (a) continuous CNTs and (b) discontinuous CNTs.

high crosslink density systems, several nearby crosslink sites may result in a void opening in the CNT surface enabling the crosslinked CNT atoms to remain $sp^2$ by breaking a CNT-CNT bond.

To better understand the statistical scatter between models, two independent systems were created at each crosslinking fraction, resulting in a total of 20 independent simulated systems. The two independent discontinuous systems were created with different CNT translations resulting in different spacing of neighboring CNT ends.

All systems are composed of fourteen CNTs and a matrix of AC with an AC:CNT mass ratio of 167:100. After equilibration, the AC matrix for each system is near 2.4 $g/cm^3$, which is within the range of experimentally produced AC [11]. For the discontinuous systems, the size of the simulation box, spacing between CNT bundles, and mass ratio were set to match the continuous systems, which results in slightly lower final AC densities, near 2.2 $g/cm^3$, due to the additional 2 nm gap added between CNT end-caps. The composites have a CNT volume fraction near 50%. The equilibrated composite densities are around 1.75 $g/cm^3$.

Each system was created independently using an equilibration procedure that lasts for 607 ps. The equilibration procedure involves minimizing the system for 32 ps at low temperature, heating the system to 1,200 K in 60 ps, maintaining the system at 1,200 K for 150 ps, and then cooling the system to 300 K in 90 ps. This is followed by two 110 ps heating and cooling cycles. Additional details on the equilibration procedure may be found elsewhere [12].

Elastic properties were predicted based on the equivalent continuum method[13] where stresses and strains are related via the stiffness tensor. Each system was strained 0.25%, 0.50%, and 1.00%, and the resulting stiffness tensors averaged. The stiffness tensor of the composite constituents was computed from the constituent stress difference between the strained and unstrained systems and the composite box strain. Since composite strains are used and not constituent strains, the properties reported here are considered in-situ values that reflect the stress transfer within the system.

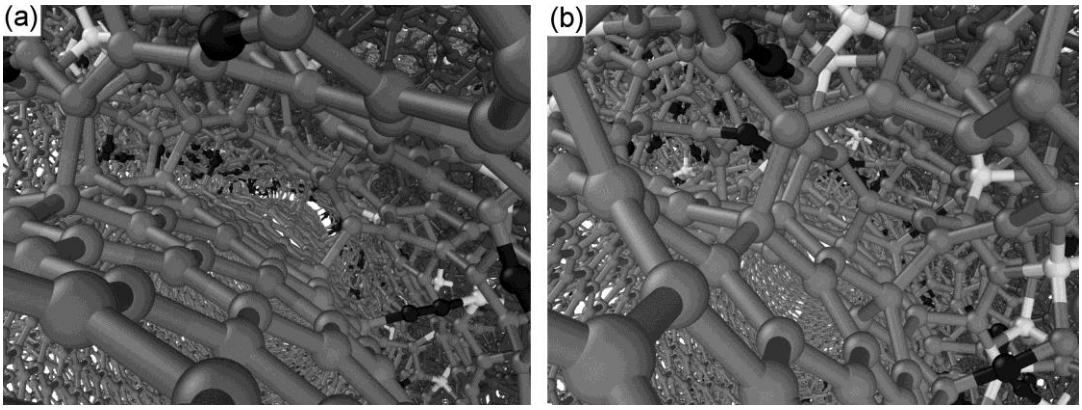

Figure 2 – CNT-AC crosslinks in the (a) 4% and (b) 19% crosslinked discontinuous systems.

The ultimate strength was predicted by straining each system in uniaxial tension. Poisson contraction was allowed by maintaining a pressure of zero in the transverse directions. The models were deformed at a true strain rate of 1.5 $ns^{-1}$ using a time step of 0.2 fs. The strain rate and time step were selected based on previous studies of AC and CNTs using the $ReaxFF_{C\text{-}2013}$ parameters.[8, 12] The ultimate tensile strength is averaged over the preceding 2 ps to reduce the effects of instantaneous thermal fluctuations.

In this work, all mechanical properties will be reported in specific units of $GPa/(g/cm^3)$, which is volume independent and can be reduced to N/(g/km). The units of $GPa/(g/cm^3)$ are equivalent to N/tex units, which are common in the fiber industry. Specific stress therefore represents only the inherent atomic bond stresses and neglects contributions that originate solely from changes in density of the material, which can be substantial in high void content materials like CNTs.

## RESULTS

### Interface Structuring

Structuring in the matrix at the interface with the CNTs was observed in the systems. Examples of this are shown in Figure 3(a) and Figure 3(b) of <1% crosslinked continuous and discontinuous systems, respectively, in which the CNTs have been hidden to reveal the matrix interface surface topography. The interface surface is composed of a mix of ring sizes and resembles a highly defective CNT. The surface of the discontinuous system appears less structured than the continuous system.

The matrix interfacial structuring can be further characterized by computing cylindrical distribution functions, shown in Figure 4. The cylindrical distribution function is computed in a similar fashion as the more common radial distribution function but with cylindrical shells radiating outward from the center of mass of each of the exterior CNTs in the bundles. The cylindrical distribution functions for the discontinuous systems are computed only along the middle length of the selected CNT, terminating before the end-caps, as shown in Figure 4(a). Therefore the end-caps and matrix gap between the ends are excluded from the calculation.

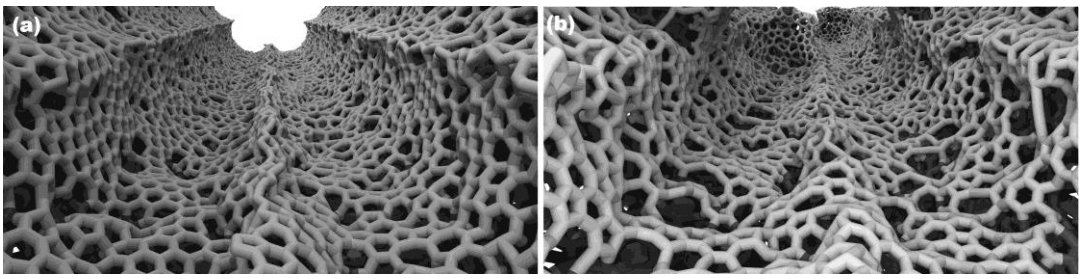


Figure 3 – "Down the barrel" view of the matrix interface surface of (a) <1% crosslink continuous and (b) <1% crosslink discontinuous systems. CNT atoms have been hidden.

However, neighboring CNT end-caps and AC gaps are still included in the computation. These exclusions make the discontinuous CNT cylindrical distribution function comparable to the continuous systems. The zero radius point in Figure 4(b) is set to correspond to the CNT wall. Looking at Figure 4(b), the first peak in the matrix at ~0.34 nm corresponds to the interface layer. The magnitude of this peak is smaller in the discontinuous system for the matrix. There is a smaller peak at approximately 0.68 nm, after which the cylindrical distribution function plateaus. Preliminary investigations found that the mechanical properties at the second 0.68 nm peak did not substantially differ from the bulk matrix and were therefore included in the bulk matrix component in subsequent computations.

From observation of the matrix interface in Figure 3 and the computed cylindrical distribution function in Figure 4, it is apparent that the interface is less structured in the discontinuous systems than in the continuous systems. There are several factors that may contribute to the decreased structuring. One possibility is that neighboring CNT ends are disrupting the crystallization of the interface. Another factor is that the discontinuous CNTs are not as straight as the continuous CNTs since there are larger wavelength deformations available to the discontinuous CNTs. The periodicity of the continuous CNTs limits the largest wavelength deformation to the length of the box. The interface structuring shown in Figure 3 and characterized in Figure 4 influences the mechanical properties as discussed later.

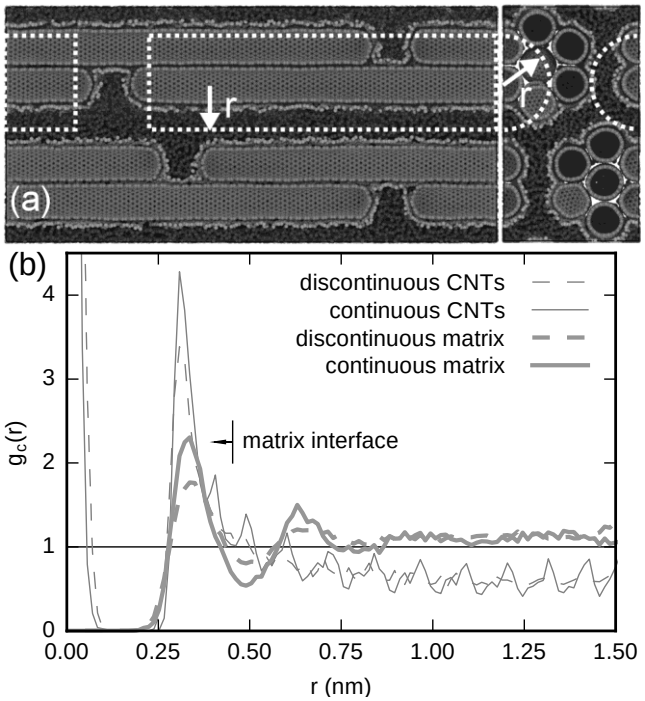


Figure 4 – (a) schematic of cylindrical computation for a discontinuous system, (b) cylindrical distribution function comparing <1% crosslinked discontinuous and continuous systems.

**Elastic Properties**

The axial specific moduli of the composites are shown in Figure 5(a). Looking at the discontinuous system, the lowest crosslinking composite axial specific modulus is on the order of the matrix stiffness. The composite axial specific modulus increases 21%, from <1% to 4% crosslinking. The maximum axial specific modulus is achieved between 4% and 7% crosslinking at 131 and 133 GPa/(g/cm$^3$), respectively, where load transfer to the CNTs is optimized. Above 7% crosslinking, the enhanced load transfer to the tubes is more than offset by degradation of the CNT and matrix interface resulting in decreasing composite specific stiffness. In the highest crosslink system, the composite axial specific modulus is 10% higher than the <1% crosslinked system.

Looking now at the continuous CNT composite in Figure 5(a), the axial specific modulus continually decreases with crosslinking, from the maximum at <1% crosslinking of 205 GPa/(g/cm$^3$). In the continuous systems, the properties of the composite are dominated by the properties of the CNTs, which degrade with crosslinking, because load transfer between the CNTs and matrix is not required. The maximum crosslink composite axial specific modulus is 22% lower than the <1% crosslinked system.

The composite axial specific moduli in Figure 5(a) are broken down into their constituents: continuous system constituents in Figure 5(b), and discontinuous system constituents in Figure 5(c). The moduli of the constituents are computed using composite strains and not constituent strains. Therefore, the constituent properties represent the stress transfer to the constituents. Looking first at the continuous CNT constituents in Figure 5(b), there is a decrease in the stiffness of both the CNTs and interface layer as crosslinking increases, resulting in lower composite stiffness. This is because the crosslinks act effectively as defects in the otherwise crystalline sp$^2$ CNT structure. The CNT stiffness decreases 21% from

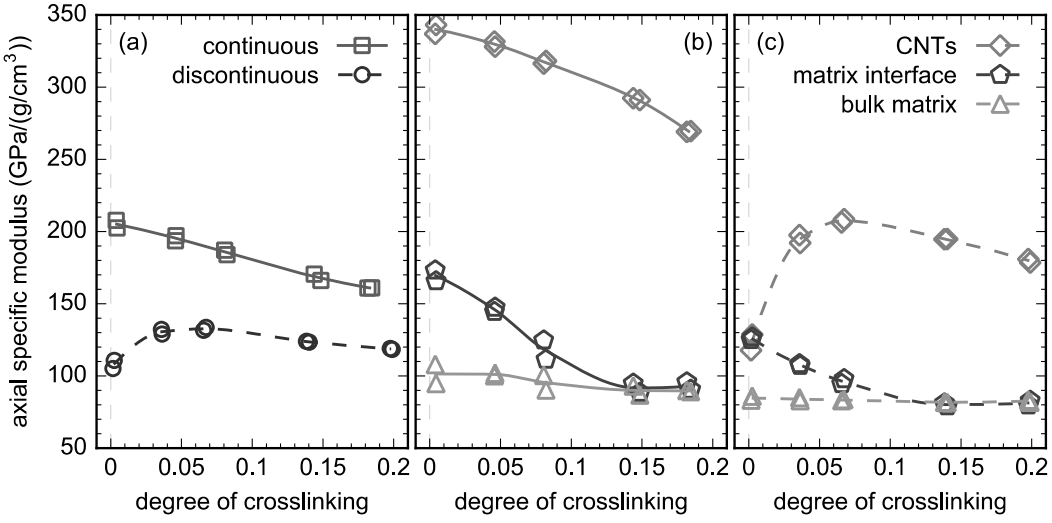


Figure 5 –Axial specific modulus of (a) composites, (b) continuous CNT constituents, and (c) discontinuous CNT constituents as a function of degree of crosslinking. (b) and (c) share the same legend.

340 to 269 GPa/(g/cm$^3$). The decrease in interfacial stiffness is due to disruption of the atomic structuring, seen previously in Figure 2(c), by the crosslinks. At <1% crosslinking, the interface layer is 68% higher than the bulk matrix. The interface stiffness decreases 46% from 170 to 92 GPa/(g/cm$^3$) from <1% to 15% crosslinking. For the two highest crosslinking fractions of 15% and 18% , the interface is totally disrupted and has properties similar to the bulk matrix. The bulk matrix decreases slightly, 12%, between <1% and 18% crosslinking, which is likely due to a small amount of structuring in the bulk matrix beyond the interface layer, seen previously in Figure 4.

Finally, the constituents of the discontinuous systems are shown in Figure 5(c). As expected, the CNTs have the lowest stiffness in the <1% crosslinked systems. It is surprising that the CNTs experience any stress in the <1% crosslinked systems, since van der Waals interactions and a very small number of crosslinks are the only method of stress transfer. One of the <1% crosslinked systems was tested again, after the small number of crosslinks were manually removed, but this did not significantly reduce the CNT stress. It is possible that this is due to a mismatch in the Poisson's ratio of the matrix and CNT causing the matrix to squeeze the CNT, resulting in an axial stress. As crosslinking increases, the CNT stiffness increases to a maximum at 7% crosslinking of 207 GPa/(g/cm$^3$). It is observed however, that the central CNT in the bundles has negligible stress in all the simulations. If the central CNT is excluded from the CNT stress average, then discontinuous CNT stresses can be multiplied by 7/6 to get the average outer CNT stress. This results in an axial CNT specific stiffness of 242 GPa/(g/cm$^3$) with optimal crosslinking, which is 71% that of the maximum CNT stress, found for <1% crosslinked continuous CNTs. With additional crosslinking beyond 7%, any increased load transfer is more than offset by damage to the CNTs. The CNT axial specific modulus at the highest crosslinking, 20%, is reduced 13% from the optimum 7% crosslink system.

Similarly to the continuous systems, the interface layer has a 48% higher stiffness at low crosslinking fractions than the bulk matrix. As was previously discussed, the discontinuous system interface is less structured than the continuous system, resulting in a lower axial specific stiffness. As crosslinks are added, the interface structure is disrupted until the stiffness is similar to the bulk matrix for the highest two crosslinked fractions. The stiffness of the interface in the <1% crosslinked discontinuous system is 26% lower than the corresponding continuous system. This is a result of the decreased structuring shown in the cylindrical distribution function shown in Figure 4. This could also be influenced by the interface around the end-caps that are not aligned in the axial direction, and therefore contribute less to axial stiffness. The tradeoff between increased CNT load transfer and decreased interfacial stiffness in Figure 5(c) results in the plateauing of the discontinuous CNT composite axial specific modulus between 4% and 7% crosslinking in Figure 5(a).

**Fracture Properties**

The axial ultimate stress as a function of crosslinking is shown in Figure 6. The composite ultimate stresses are shown in Figure 6(a). The continuous composite axial ultimate specific stress decreases 17% from 32 to 27 GPa/(g/cm$^3$) from <1% to 18% crosslinking. The discontinuous ultimate stress increases 85% from 12 to 22

GPa/(g/cm$^3$). The difference in CNT specific ultimate stress between the highest crosslinked continuous and discontinuous systems is 5 GPa/(g/cm$^3$), with the discontinuous system 19% lower. Additional crosslinking above 15% does not affect the specific ultimate stress of either continuous or discontinuous systems. This differs from the axial specific modulus, discussed earlier, which is maximized at 4-7% crosslinking for the discontinuous system, after which additional crosslinks decrease the modulus. As discussed in the introduction, the continuous and discontinuous systems represent maximum and minimum cases, respectively. Composites composed of large aspect ratio CNTs are expected to have properties that lie between these two simulated cases.

The ultimate specific stresses experienced by the composite constituents are shown in Figure 6(b) and Figure 6(c) for continuous and discontinuous systems, respectively. In both continuous and discontinuous systems, the bulk matrix has a specific ultimate stress around 18 GPa/(g/cm$^3$). Looking at the continuous systems, both the CNT and interface layer are continuously decreased by increased crosslinking. The CNT axial specific ultimate stress decreases 32% from 58 to 39 GPa/(g/cm$_3$) from the <1% to 18% crosslinked systems. Similarly, the matrix interface decreases 30% from <1% to 15% crosslinking, after which the matrix interface ultimate stress plateaus. In the <1% crosslinked system, the matrix interface has an axial ultimate specific stress 50% higher than the bulk matrix.

For discontinuous systems, shown in Figure 6(c), the CNTs have a negligible ultimate specific stress at <1% crosslinking, which increases up to 14% crosslinking at 28 GPa/(g/cm$^3$), after which there is no further improvement in CNT ultimate specific stress. Similarly to the continuous systems, the ultimate specific stress of the interface layer in the discontinuous systems continuously decreases with increased crosslinking and becomes comparable to the bulk matrix by 14% crosslinking. In the <1% crosslinked system, the interface layer has an axial ultimate specific stress of 23 GPa/(g/cm$^3$), which is 35% stronger than the bulk matrix.

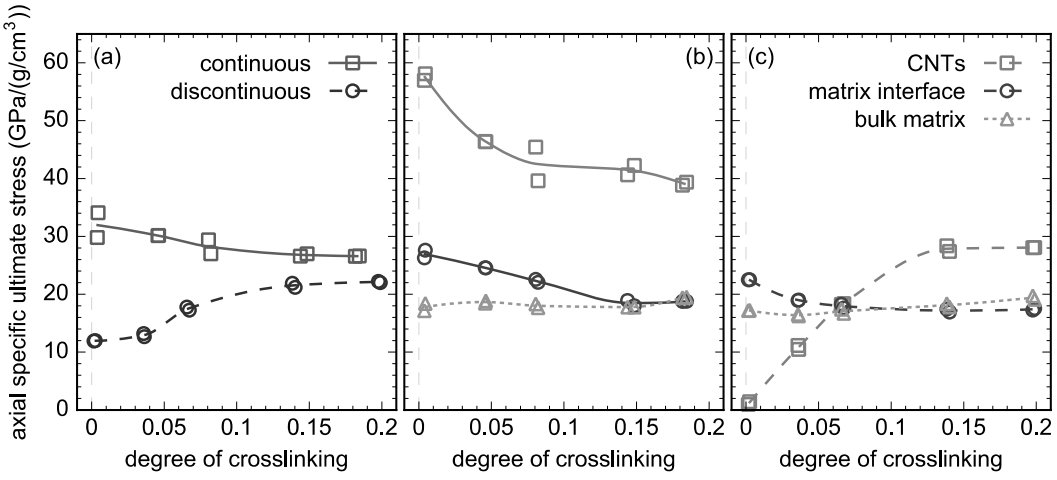


Figure 6 – Comparison of discontinuous and continuous CNT axial specific ultimate stresses for (a) overall composite response (b) continuous CNT composite constituents, and (c) discontinuous CNT composite constituents. (b) and (c) share the same legend.

**Mechanical Performance Summary**

To compare the elastic and fracture response properties of discontinuous and continuous CNTs, the axial specific modulus and ultimate stress are plotted in Figure 7. For each label, five points are plotted corresponding to the five crosslinking fractions. Arrows indicate the direction of increasing crosslinking. The discontinuous system properties are plotted with dashed lines and continuous CNT properties with solid lines. Both the composite and the in-situ constituent properties are shown. CNT properties are marked with triangles, and composite properties with circles. Since the bulk matrix properties did not significantly vary with crosslinking or CNT continuity, all of the bulk matrix values have been averaged and the result plotted with a black square. The matrix interface properties are not shown to reduce clutter on the figure, but were seen previously to have properties similar to the final composite.

The composite, CNT constituents, and bulk matrix constituent axial specific modulus and ultimate stress in Figure 7 have been shown previously in Figure 5 and Figure 6, respectively. Figure 7 allows for easier comparison of the elastic and fracture properties. Looking at the continuous systems, both the axial specific modulus and specific ultimate stress decrease with the addition of crosslinks. In the discontinuous systems, this is inverted for the specific ultimate stress, the addition of crosslinks increases the specific ultimate stress over the range of crosslinks. However, in the discontinuous systems, the axial specific modulus is optimized at moderate crosslinking, between 4%-7%, and further increases in crosslinking above 7% decrease the axial specific modulus. It is important to note for design of these materials that optimized levels of crosslinking may be different for fracture and elastic properties.

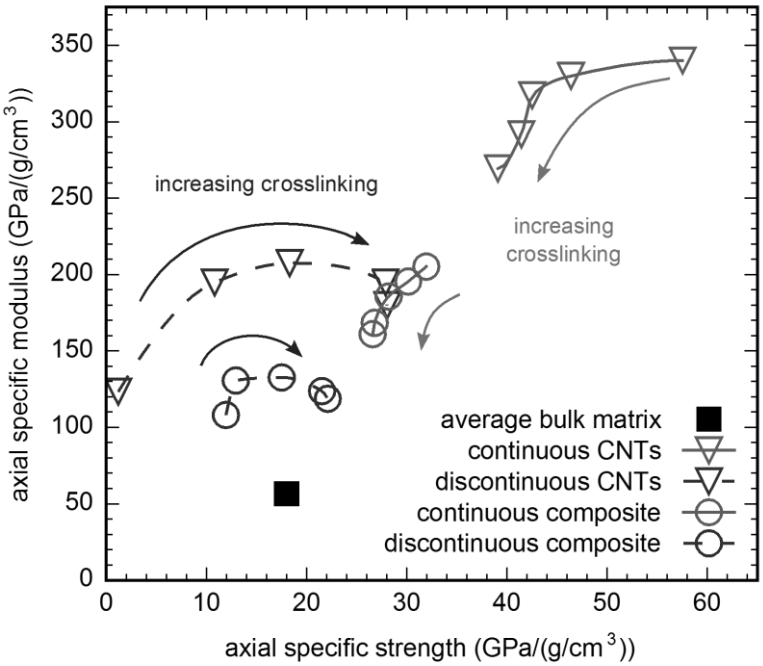


Figure 7 – Comparison of composite and constituent specific axial modulus and strength. The matrix interface is not shown.

## CONCLUSIONS

Molecular dynamics models of continuous and discontinuous CNT/AC composite systems were modeled with CNT-matrix covalent crosslinking fractions ranging from 0-20%. The CNTs were arranged into two bundles of seven CNTs each. These models were strained both elastically and to failure and the elastic constants and ultimate stresses were computed. The discontinuous CNTs modeled herein have an aspect ratio orders of magnitude smaller than those found in current CNT yarns and sheets. Therefore, these systems represent a lower bound, while the continuous systems represent an upper bound for mechanical properties. Additional features of CNT materials beyond the scope of this work, such as meso-scale structuring and micro-sized voids, are expected to further reduce the mechanical properties reported here.

Structuring of the matrix at the CNT interface was observed and characterized through a cylindrical distribution function. The interface was found to be composed of aromatic rings and with a density peak around 0.34 nm from the CNT wall and extended to a maximum around 0.45 nm. The interface layer was found to have 48-68% higher axial specific stiffness and 35-50% higher ultimate stress than the bulk matrix in the <1% crosslinked systems. As crosslinking increases, the mechanical properties of the interface layer decrease until they become equal to the bulk matrix at 15% crosslinking.

The composite axial elastic modulus is maximized between 4%-7% crosslinking with 133 GPa/(g/cm$^3$) for discontinuous systems, and at <1% crosslinking with 205 GPa/(g/cm$^3$) for continuous systems. The maximized discontinuous CNT specific axial modulus is 71% that of maximized continuous CNTs.

The axial ultimate tensile stress continually increases with crosslinking in the discontinuous systems, to a maximum of 22 GPa/(g/cm$^3$) at 20% crosslinking. Conversely, the continuous system's axial ultimate stress continually decreases with crosslinking form a maximum of 32 GPa/(g/cm$^3$) in the <1% crosslinked system to a minimum of 27 GPa/(g/cm$^3$) in the 18% crosslinked system. The strength of discontinuous systems approach 70% of the continuous systems at the highest crosslinking fractions.

## REFERENCES


1. Li, Y.-L., I. A. Kinloch. A. H. Windle. 2004. "Direct spinning of carbon nanotube fibers from chemical vapor deposition synthesis," *Science 304* (5668):276-278.
2. Motta, M., A. Moisala, I. A. Kinloch. A. H. Windle. 2007. "High performance fibres from 'dog bone'carbon nanotubes," *Adv. Mater. 19* (21):3721-3726.
3. van Duin, A. C. T., S. Dasgupta, F. Lorant. W. A. Goddard, III. 2001. "ReaxFF: A reactive force field for hydrocarbons," *J. Phys. Chem. A 105* (41):9396-9409.
4. Goverapet Srinivasan, S., A. C. T. van Duin. P. Ganesh. 2015. "Development of a ReaxFF potential for carbon condensed phases and its application to the thermal fragmentation of a large fullerene," *J. Phys. Chem. A 119* (4):571-580.
5. Plimpton, S. 1995. "Fast parallel algorithms for short-range molecular-dynamics," *J. Comput. Phys. 117* (1):1-19.
6. Aktulga, H. M., J. C. Fogarty, S. A. Pandit. A. Y. Grama. 2012. "Parallel reactive molecular dynamics: Numerical methods and algorithmic techniques," *Parallel Comput. 38* (4-5):245-259.

7. Senftle, T. P., S. Hong, M. M. Islam, S. B. Kylasa, Y. Zheng, Y. K. Shin, C. Junkermeier, R. Engel-Herbert, M. J. Janik. H. M. Aktulga. 2016. "The ReaxFF reactive force-field: Development, applications and future directions," *npj Computational Materials 2* 15011.
8. Jensen, B. D., K. E. Wise. G. M. Odegard. 2015. "Simulation of the elastic and ultimate tensile properties of diamond, graphene, carbon nanotubes, and amorphous carbon using a revised reaxff parametrization," *J. Phys. Chem. A 199* (37):9710–9721.
9. Alexander, S. 2010. "Visualization and analysis of atomistic simulation data with Ovito–the open visualization tool," *Modell. Simul. Mater. Sci. Eng. 18* (1):015012.
10. Hunter, J. D. 2007. "Matplotlib: A 2D graphics environment," *Computing in Science & Engineering 9* (3):90-95.
11. Ferrari, A. C., A. Libassi, B. K. Tanner, V. Stolojan, J. Yuan, L. M. Brown, S. E. Rodil, B. Kleinsorge. J. Robertson. 2000. "Density, $sp^3$ fraction, and cross-sectional structure of amorphous carbon films determined by x-ray reflectivity and electron energy-loss spectroscopy," *Phys. Rev. B 62* (16):11089-11103.
12. Jensen, B. D., K. E. Wise. G. M. Odegard. 2016. "Simulation of mechanical performance limits and failure of carbon nanotube composites," *Modell. Simul. Mater. Sci. Eng. 24* (2):025012.
13. Odegard, G. M., T. S. Gates, L. M. Nicholson. K. E. Wise. 2002. "Equivalent-continuum modeling of nano-structured materials," *Compos. Sci. Technol. 62* (14):1869-1880.